

Constraining low-scale dark phase transitions with cosmological observations

Shihao Deng¹ and Ligong Bian^{1,2*}

¹*Department of Physics, Chongqing University, Chongqing 401331, China* and

²*Center for High Energy Physics, Peking University, Beijing 100871, China*

We investigate the effects of the low-scale cosmological first-order phase transitions on the neutrino decoupling and constrain the PT parameters with the cosmological observations of big bang nucleosynthesis and cosmic microwave background. We consider the phase transitions that occur at the MeV-scale which can produce stochastic gravitational wave background to be probed by pulsar timing array experiments. We find that the phase transition can modify the effective number of neutrinos and the primordial nucleosynthesis. In turn, the cosmological observations can exclude slow and strong phase transitions around the MeV scale.

INTRODUCTION

The cosmological first-order phase transitions (PTs) are generally predicted by many well-motivated new physics models [1–4]. The first-order PTs are expected to produce stochastic gravitational wave background (SGWB) [5, 6], explain the source of primordial magnetic fields [7, 8] and the origin of the baryon asymmetry of the Universe [9]. The SGWB produced by the first-order PTs is one of the main scientific goals of many gravitational detectors, such as LIGO [10, 11], LISA [12], *Taiji* [13], NANOGrav [14], PPTA [15], and SKA [16]. Since both the types of the electroweak PT and the QCD PT in the Standard Model of particle physics are *cross-over* [17, 18], observing the SGWB relics of the first-order PTs would help to probe the parameters of new physics beyond the Standard model [5, 6, 19–21].

The low-scale first-order PTs can occur in QCD when lepton asymmetry shows up [22–25], and thermal dark sectors [26]. MeV-scale dark matter is of great interest since it is highly connected with the neutrino decoupling process, and therefore the cosmic microwave background (CMB) and Big Bang nucleosynthesis (BBN) [27–30]. Recently, the constraints on MeV-scale dark matter have been drawn by Ref. [29, 31, 32] after considering detailed thermal dynamics in the early Universe. Ref. [33] shows that the vacuum energy from the first-order PTs can yield photon reheating and/or neutrino reheating, which would change the effective number of neutrinos. It was also observed that the appearance of the first-order PTs would change the time-temperature relation in the early universe, and therefore affect the light-element abundance during the BBN process.

In this work, we consider the effects of the MeV-scale first-order PTs on the CMB and BBN when the MeV-scale thermal dark sector was taken into account. We include the dynamics of the PTs on the evolution of time and temperature around the MeV-scale at the early universe to study the neutrino decoupling process and the BBN process. We then place constraints on PTs parameters with the corresponding cosmological observations of CMB and BBN.

THERMAL DYNAMICS WITH FIRST-ORDER PTS

Before PTs, we assume that all particle species are in thermal equilibrium, and are described by a thermal equilibrium distribution function, characterized by a temperature T_i . First-order PTs proceed through true vacuum bubbles nucleation and percolation with the nucleation rate [34, 35]: $\Gamma(t) = \Gamma_0 e^{\beta t}$, where the β characterizes the PT rate or the true vacuum bubbles nucleations rate, and pre-factor can be estimated as [36] $\Gamma_0^{1/4} = (4\pi^3 g_*/45)^{1/2} (T_p^2/m_{\text{Pl}}) e^{-\beta/8H_*}$ in the radiation dominant universe with T_p being the PT temperature and H_* being the Hubble parameter at the PT temperature, the Planck mass is $m_{\text{Pl}} = 1.22 \times 10^{19} \text{ GeV}$. At the PT time, the PT's inverse duration is $\beta/H_* \equiv \beta/H(t_p)$ and the PT's strength is $\alpha \equiv \Delta V/\rho_r(t_p)$ where ΔV denotes the energy density difference between the false and true vacua. We consider the PT occurs as the averaged probability of the false vacuum $F(t_p) = 0.7$. The $F(t)$ can be calculated through [37] $F(t) = \exp \left[-\frac{4\pi}{3} \int_{t_i}^t dt' \Gamma(t') a^3(t') r^3(t, t') \right]$, where t_i is the time when PTs starts and $r(t, t') \equiv \int_{t_i}^t a^{-1}(\tau) d\tau$ is the comoving radius of true vacuum bubbles. Before PTs, all the fields settle in the false vacuum with $F(t < t_i) = 1$.

Considering the case of photon reheating driven by the first-order PTs, we study the early thermodynamics of the universe with MeV-scale thermally electrophilic dark sectors. More explicitly, we extend the corresponding temperature evolution equations given in Ref [30] to include the PTs dynamics,

$$\begin{aligned} \frac{dT_\nu}{dt} &= - (12H\rho_\nu - \frac{\delta\rho_{\nu_e}}{\delta t} - 2\frac{\delta\rho_{\nu_\mu}}{\delta t})/(3\frac{\partial\rho_\nu}{\partial T_\nu}), \\ \frac{dT_\gamma}{dt} &= - \left(4H\rho_\gamma + 3H(\rho_e + p_e) + 3H(\rho_\chi + p_\chi) \right. \\ &\quad \left. + 3H T_\gamma \frac{dP_{\text{int}}}{dT_\gamma} + \frac{\delta\rho_{\nu_e}}{\delta t} + 2\frac{\delta\rho_{\nu_\mu}}{\delta t} + \frac{d\rho_{\text{vac}}}{dt} \right) / f(T_\gamma). \end{aligned} \quad (1)$$

Here, $f(T_\gamma) = \frac{\partial\rho_\gamma}{\partial T_\gamma} + \frac{\partial\rho_e}{\partial T_\gamma} + \frac{\partial\rho_\chi}{\partial T_\gamma} + T_\gamma \frac{d^2 P_{\text{int}}}{dT_\gamma^2}$, and the energy

exchange rates $\delta\rho_{\nu_e}/\delta t$ and $\delta\rho_{\nu_\mu}/\delta t$ are:

$$\begin{aligned}\frac{\delta\rho_{\nu_e}}{\delta t} &= \frac{G_F^2}{\pi^5} \left[(1 + 4s_W^2 + 8s_W^4) F(T_\gamma, T_{\nu_e}) + 2F(T_{\nu_\mu}, T_{\nu_e}) \right], \\ \frac{\delta\rho_{\nu_\mu}}{\delta t} &= \frac{G_F^2}{\pi^5} \left[(1 - 4s_W^2 + 8s_W^4) F(T_\gamma, T_{\nu_\mu}) - F(T_{\nu_\mu}, T_{\nu_e}) \right],\end{aligned}\quad (2)$$

with $F(T_1, T_2) = 32(T_1^9 - T_2^9) + 56T_1^4T_2^4(T_1 - T_2)$, and where $G_F = 1.1664 \times 10^{-5}$ GeV $^{-2}$ is the Fermi constant, and $s_W^2 = 0.223$ accounts for the Weinberg angle [38]. Finite temperature corrections and its derivatives are accounted for by P_{int} [30]. In the above equations, ρ_i and p_i correspond to the energy density and pressure of a given particle respectively, $H = \sqrt{(8\pi/3)(\sum_i \rho_i + \rho_{\text{vac}})/m_{\text{Pl}}^2}$ is the Hubble parameter. The $\rho_{\text{vac}} = F(t)\Delta V$ is the energy density of the false vacuum.

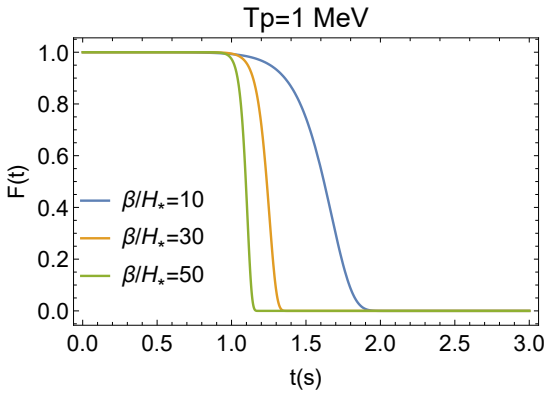


FIG. 1. $F(t)$ as a function of t , for $\beta/H_* = 10, 30$, and 50 , respectively.

As the false vacuum decay occurs in the expanding Universe, the energy density becomes larger after a PT since ρ_γ decrease as a^{-4} while ΔV remains almost constant. As the PT proceeds, $F(t)$ decreases, and the false vacuum energy transfers into the background plasma and yields photon reheating, causing an increase in their temperature and a subsequent decrease in $N_{\text{eff}} = 3 \times (11/4)^{4/3} (T_\nu/T_\gamma)^4$. The effect of T_p is significant, as it impacts mainly include two aspects: the PT strength α and the time at which $F(t)$ takes effect in the neutrino decoupling process. Around 0.8 MeV, the neutrinos decouple, so the injection of PT's energy around this time will have a significant effect on N_{eff} . As shown in Fig. 1, the value of $F(t)$ changes much faster for a larger value of β/H_* at the fixed PT temperatures. For $T_p = 1$ MeV, $F(t)$ starts to fall just around 1s, which has a significant effect on neutrino decoupling. As T_p increases, the magnitude of the $F(t)$ would decrease earlier, and thus the effect on neutrino decoupling will be weaker, so N_{eff} decreases even less compared to the Standard Model.

The observed DM abundance in the Universe can be explained by a WIMP particle that annihilates to light

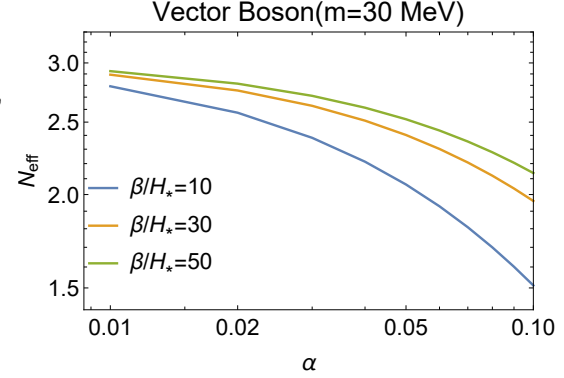


FIG. 2. N_{eff} as a function of α , for $\beta/H_* = 10, 30$, and 50 , respectively.

species at a rate of $\langle\sigma v\rangle \simeq 3 \times 10^{-26}$ cm 3 /s [39]. Such a particle would decouple from the plasma while non-relativistic at temperatures of $T \sim m/20$, and for WIMPs of $m \lesssim 20$ MeV, neutrino decoupling and N_{eff} would be affected. However, if the DM mass is greater than 20 MeV, the effect on neutrino decoupling would be negligible, and N_{eff} would be very close to the Standard Model value. For a vector boson with a mass of 30 MeV, N_{eff} is calculated to be 3.04335, which is close to the Standard Model value. Therefore, to capture the dynamics and effects of the PTs, we consider the dark sector with mass being fixed at 30 MeV. We, therefore, solve the time evolution equations for T_γ and T_ν starting from $T_\gamma = T_\nu = 30$ MeV, since for such high temperatures SM neutrino-electron interactions are highly efficient. The starting time for the evolution is simply $t = 1/(2H)$, which corresponds to $t_0 \sim 7 \times 10^{-4}$ s, and we evolve the system until $t_{\text{final}} = 5 \times 10^4$ s where the electrons and positrons have already annihilated away. By solving this set of differential equations, we can find all the key background evolution quantities as a function of time, scale factor, and temperature. Technically, we modify the publicly available versions of NUDEC_BSM [30, 32] to take into account the PT dynamics, and use it to compute the background thermodynamics and N_{eff} , which is crucial for CMB observations. Fig. 2 illustrates the impact of two PT parameters (α and β/H_*) on N_{eff} with the PT temperature being $T_p = 1$ MeV for the scenario of vector boson mass $m = 30$ MeV, which depicts that, for the fixed PT duration time, the increase of PT strength (α) results in the decrease of N_{eff} .

In the top two plots of Fig. 3, we present the effect of T_p and β/H_* on the effective number of neutrinos N_{eff} is shown for different α . Roughly speaking, when $T_p \sim 4$ MeV, the value of N_{eff} is already within the 1σ error range allowed by Planck dataset [40]. In the bottom two plots of Fig. 3, we demonstrate the joint effect of α and β/H_* on N_{eff} for different T_p . The effect of the PTs is greater for the scenario of $T_p = 1$ MeV than that of

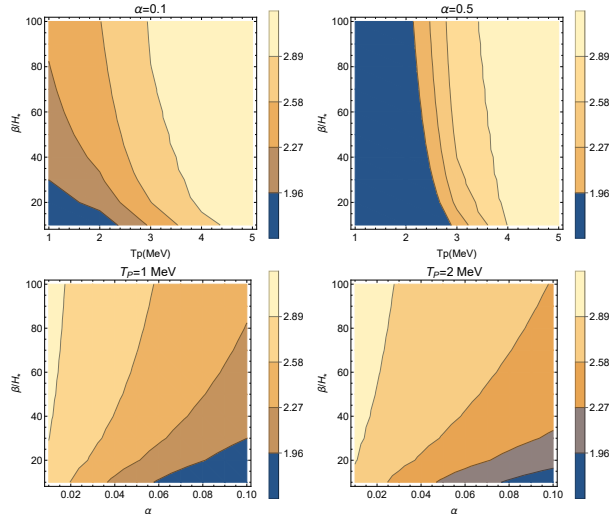


FIG. 3. The top-left and top-right panels show the effect of T_p and β/H_* on N_{eff} for $\alpha = 0.1$ (top-left) and $\alpha = 0.5$ (top-right). Here, 2.89 is the central value of N_{eff} in the Planck dataset, and the numbers 2.58, 2.27, and 1.96 correspond to the error range of 1σ , 2σ , and 3σ , respectively. The bottom-left and bottom-right panels show the effect of α and β/H_* on N_{eff} for different T_p , where we set $T_p = 1 \text{ MeV}$ (bottom-left) and $T_p = 2 \text{ MeV}$ (bottom-right).

$T_p = 2 \text{ MeV}$.

PRIMORDIAL NUCLEOSYNTHESIS AND FIRST-ORDER PTS

Conventionally, the neutron fraction $X_n \equiv n_n/n_b$, which represents the ratio of neutron number density to baryon number density, is a crucial intermediate quantity in BBN. When the temperature is high, neutrons and protons transform into each other through $n \leftrightarrow p$ reactions and these weak interactions are in equilibrium. Neglecting the chemical potential of electrons and neutrinos, the equilibrium abundance of neutrons is $X_n^{\text{eq}} = e^{-Q/T}/(1 + e^{-Q/T})$, where $Q \equiv m_n - m_p = 1.293 \text{ MeV}$. The neutrons follow a thermal equilibrium distribution until neutrinos decouple at around $T_{\text{FO}} \sim 0.8 \text{ MeV}$ ($t_{\text{FO}} \sim 1 \text{ s}$).

After the freeze-out, X_n slowly decreases due to occasional weak reactions and is eventually dominated by free neutron decay. During this time, neutrons decay into protons, and the remaining fraction of neutrons is given by $X_n(t > t_{\text{FO}}) \approx X_n(t_{\text{FO}})e^{-t/\tau_n}$. As the temperature of the Universe falls to the nucleosynthesis temperature of $T_{\text{nuc}} \approx 0.078 \text{ MeV}$ (at time t_{nuc}), the production of helium begins and the fraction Y_p starts to increase. The final abundance of Y_p is determined by the abundance of neutrons at the onset of nucleosynthesis, which is given by $X_n(t_{\text{nuc}})$, and is approximately $Y_p \approx 2X_n(t_{\text{nuc}})$.

First-order PTs can have an impact on both CMB and BBN if the temperature of the first-order PT is low-scale around MeVs. When the low-scale first-order PTs happen, the process of photon reheating affects the time-temperature relation. For a given photon temperature, the total energy density and the Hubble rate decrease so is the rate of variation dT/dt . This means that the onset of nucleosynthesis will occur much later, i.e., t_{nuc} is delayed, resulting in a smaller final Y_p .

On the other hand, in the case of a first-order PT with photon reheating, the neutrino temperature is lower than in the absence of a PT, resulting in a decrease in both the neutrino density and the weak reaction rate Γ_{np} at a given $T = T_\gamma$, which can lead to an earlier freeze-out, with larger neutron fraction $X_n(T_{\text{FO}}) \approx X_n^{\text{eq}}(T_{\text{FO}})$. However, the reduced neutrino density also leads to a decrease in the Hubble rate, which partially offsets the effect on Γ_{np} [41]. The correction of the weak rate Γ_{np} is more significant due to its higher dependence on temperature [42]. Considering these two points together, the freeze-out temperature T_{FO} would be higher than in the absence of PTs, i.e., freeze-out occurs earlier, which probably yields a larger final Y_p . In summary, larger $X_n(t_{\text{FO}})$ tends to favor larger final Y_p while larger t_{nuc} tends to favor smaller final Y_p .

In Fig.4, we show specifically the effect of first-order PT on BBN with $T_p = 1 \text{ MeV}$, $\alpha = 0.01$ and $\beta/H_* = 10$. Compared to the absence of PT, both Y_p and $D/H|_P$ decreased. The effect of PT on $D/H|_P$ is consistent with Ref. [33], but the effect on Y_p is different, which is related to the two parameters we mentioned before, $X_n(t_{\text{FO}})$ and t_{nuc} . In our case, the effect of t_{nuc} is a little stronger than $X_n(t_{\text{FO}})$ and leads to a decrease in Y_p , however, in the case of Ref. [33], the effect of $X_n(t_{\text{FO}})$ is stronger than t_{nuc} and finally leads to a larger Y_p .

Deuterium is formed directly from neutrons and protons and its abundance follows the equilibrium value as long as there are plenty of free neutrons available. Thus, the freeze-out has almost no impact on the abundance of deuterium. Since the deuterium binding energy is rather small, the peak of its abundance ratio occurs at around $T_{\text{nuc}} \approx 0.078 \text{ MeV}$. The primary factor that affects the abundance of deuterium is the time t_{nuc} , the reheating of photons triggered by the first-order PTs will affect the time-temperature relation, causing a later t_{nuc} , which leads to a smaller $D/H|_P$. For the calculation of the Primordial Nucleosynthesis, we pass the necessary thermodynamic parameters including T_γ , T_ν , the scale factor a , and the Hubble parameter H obtained with the modified NUDEC_BSM on to the BBN code PRIMAT [43]. These parameters were constructed as a function of time using the interpolation method and were used to replace the original thermodynamics of PRIMAT. By doing so, the time evolution of the nuclei abundances was calculated by recomputing weak interactions and nuclear reaction rates. We verified the correctness of our modified version

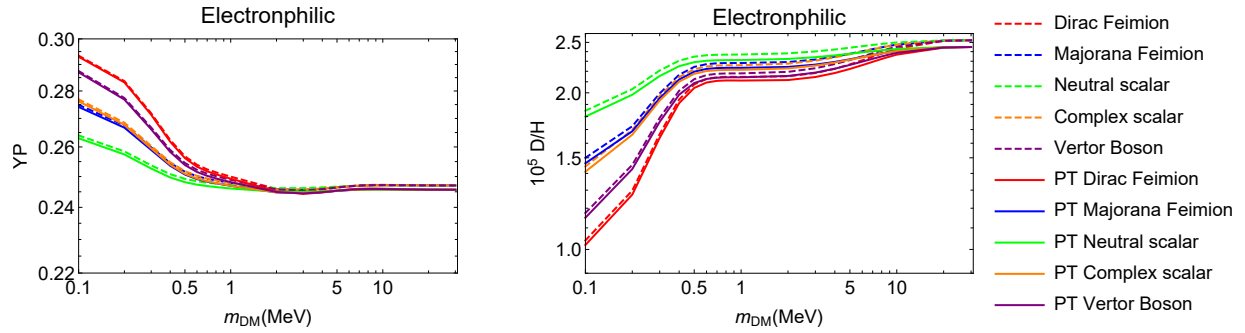


FIG. 4. Cosmological impact of light BSM particles in thermal equilibrium with the SM plasma as a function of their mass m_{DM} . The left (right) panel corresponds to Y_{P} ($D/\text{H}|_{\text{P}}$). The Y_{P} and $D/\text{H}|_{\text{P}}$ predictions are computed with $\Omega_b h^2 = 0.021875$ and $\tau_n = 879.5$ s [29]. The dashed line corresponds to the case where no PT is considered, the solid line corresponds to the scenarios with a first-order PT where $T_{\text{P}} = 1$ MeV, $\alpha = 0.01$ and $\beta/H_* = 10$.

by generating curves for the primordial helium and deuterium abundances with dark matter mass, which is in agreement with the results presented in Fig.1 of Ref. [29] when the PT dynamics were not considered.

CONSTRAINTS ON PT PARAMETERS

In this section, we study constraints on the low-scale first-order PTs from the BBN and CMB observations. For the analysis of the BBN, we consider the observation of primordial abundances of helium and deuterium (Y_{P} , $D/\text{H}|_{\text{P}}$). To obtain the current constraints on low-scale PT from BBN observables, we take the effective BBN χ^2 being [29],

$$\chi_{\text{BBN}}^2 = \frac{[Y_{\text{P}}(\Omega_b h^2, \alpha, \beta/H_*) - Y_{\text{P}}^{\text{obs}}]^2}{\sigma(Y_{\text{P}}^{\text{th}})^2 + \sigma(Y_{\text{P}}^{\text{obs}})^2} + \frac{[D/\text{H}|_{\text{P}}(\Omega_b h^2, \alpha, \beta/H_*) - D/\text{H}|_{\text{P}}^{\text{obs}}]^2}{\sigma(D/\text{H}|_{\text{P}}^{\text{th}})^2 + \sigma(D/\text{H}|_{\text{P}}^{\text{obs}})^2}. \quad (3)$$

Where, the central values are: $Y_{\text{P}}^{\text{obs}} = 0.245$, $D/\text{H}|_{\text{P}}^{\text{obs}} = 2.547 \times 10^{-5}$, and the current observational errors are $\sigma(Y_{\text{P}}^{\text{obs}}) = 0.003$, $\sigma(D/\text{H}|_{\text{P}}^{\text{obs}}) = 0.025 \times 10^{-5}$ [44], and theoretical errors are taken from Ref. [45]: $\sigma(Y_{\text{P}}^{\text{th}}) = 0.00014$, $\sigma(D/\text{H}|_{\text{P}}^{\text{th}}) = 0.037 \times 10^{-5}$. CMB observations precisely measure the value of $(\Omega_b h^2, N_{\text{eff}}, Y_{\text{P}})$, and the Gaussian likelihood for these parameters are [29]

$$\chi_{\text{CMB}}^2 = (\Theta - \Theta_{\text{obs}})^T \Sigma_{\text{CMB}}^{-1} (\Theta - \Theta_{\text{obs}}), \quad (4)$$

with $\Theta \equiv (\Omega_b h^2, N_{\text{eff}}, Y_{\text{P}})$ and

$$\Sigma_{\text{CMB}} = \begin{bmatrix} \sigma_1^2 & \sigma_1 \sigma_2 \rho_{12} & \sigma_1 \sigma_3 \rho_{13} \\ \sigma_1 \sigma_2 \rho_{12} & \sigma_2^2 & \sigma_2 \sigma_3 \rho_{23} \\ \sigma_1 \sigma_3 \rho_{13} & \sigma_2 \sigma_3 \rho_{23} & \sigma_3^2 \end{bmatrix}. \quad (5)$$

We are going to analyze with the Planck+BAO+ H_0 dataset with the experimental value of Θ being: $\Theta_{\text{obs}} = (0.02345, 3.36, 0.249)$, the parameters of the covariance

matrices are $(\rho_{12}, \rho_{13}, \rho_{23}) = (0.011, 0.50, -0.64)$ and $(\sigma_1, \sigma_2, \sigma_3) = (0.00025, 0.25, 0.020)$. The local measurement of the H_0 from the SH0ES collaboration [46] would uplift the reconstructed value of the effective number of neutrinos for some amount, for the neutrino interpretation of the Hubble Tension we refer to Ref. [47].

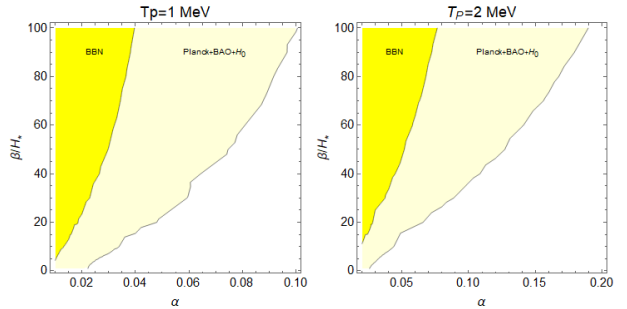


FIG. 5. The 95% CL constraints on the PT parameters α and β/H_* from CMB and BBN datasets at $T_{\text{P}} = 1$ MeV (left) and $T_{\text{P}} = 2$ MeV (right). The regions to the right of yellow and light yellow regions are excluded by the current BBN and CMB constraints respectively.

Fig. 5 displays the exclusion limits at the 95% confidence level (CL) for α and β/H_* after marginalizing over $\Omega_b h^2$. By setting $\Omega_b h^2 = 0.021875$, we obtain the minimum χ^2 value, denoted as χ_{min}^2 , and the corresponding 95% CL limits are defined by $\Delta\chi^2 = \chi^2 - \chi_{\text{min}}^2 = 5.991$. We find that: 1) strong PT of relatively large α and slow PT with small β/H_* are excluded; 2) BBN and CMB observations yield weaker constraints on PTs occurring at higher temperature (with larger T_{P}); and 3) the constraint from BBN is stronger than that of CMB for both panels, this is because that $D/\text{H}|_{\text{P}}$ provides stronger constraints compared to N_{eff} . For the PTs with $\beta/H_* = 50$, the BBN data set constrain the PT strength to be $\alpha < 0.03$ at $T_{\text{P}} = 1$ MeV and $\alpha < 0.05$ at $T_{\text{P}} = 2$ MeV.

CONCLUSION AND DISCUSSION

This study shows that, in comparison with the Standard model case, the thermal dynamics of first-order PTs lead to changes in the BBN and CMB predictions. The stronger the PTs strength and the slower the PTs, the larger deviation of the N_{eff} . And the PTs effect on the N_{eff} would be negligible when the PTs temperature $T_p > 5$ MeV. The constraints on the PTs parameter spaces from BBN are much stronger than that of the CMB, and the PTs strength of $\alpha \gtrsim \mathcal{O}(0.01-0.1)$ together with the inverse duration of $\beta/H_\star \lesssim \mathcal{O}(1-10^2)$ are excluded by the current cosmological observations at 95% CL. Nanohertz gravitational wave detection conducted by PPTA, NANOGrav, and SKA would have the chance to probe the low-scale PTs under study.

ACKNOWLEDGMENTS

We are grateful to Miguel Escudero Abenza and James Alvey for helpful discussions on the BBN code PRIMAT and the code NUDEC_BSM on the study of the neutrino decoupling. We thank Shun Zhou for insightful discussion on the relation between neutrino decoupling and low-scale phase transitions. This work is supported in part by the National Key Research and Development Program of China Grants No. 2021YFC2203004, and in part by the National Natural Science Foundation of China under grants Nos. 12075041, 12047564, 12147102, and the Fundamental Research Funds for the Central Universities of China (No. 2021CDJQY-011 and No. 2020CDJQY-Z003), and Chongqing Natural Science Foundation (Grants No.cstc2020jcyj-msxmX0814).

* lgbycl@cqu.edu.cn

- [1] M. Losada, Phys. Rev. D **56**, 2893 (1997), arXiv:hep-ph/9605266.
- [2] J. M. Cline and P.-A. Lemieux, Phys. Rev. D **55**, 3873 (1997), arXiv:hep-ph/9609240.
- [3] M. Laine, Nucl. Phys. B **481**, 43 (1996), [Erratum: Nucl.Phys.B 548, 637–638 (1999)], arXiv:hep-ph/9605283.
- [4] D. Bodeker, P. John, M. Laine, and M. G. Schmidt, Nucl. Phys. B **497**, 387 (1997), arXiv:hep-ph/9612364.
- [5] C. Caprini *et al.*, JCAP **1604**, 001 (2016), arXiv:1512.06239 [astro-ph.CO].
- [6] C. Caprini *et al.*, JCAP **03**, 024 (2020), arXiv:1910.13125 [astro-ph.CO].
- [7] T. Vachaspati, Phys. Lett. B **265**, 258 (1991).
- [8] Y. Di, J. Wang, R. Zhou, L. Bian, R.-G. Cai, and J. Liu, Phys. Rev. Lett. **126**, 251102 (2021), arXiv:2012.15625 [astro-ph.CO].
- [9] D. E. Morrissey and M. J. Ramsey-Musolf, New J. Phys. **14**, 125003 (2012), arXiv:1206.2942 [hep-ph].
- [10] J. Aasi *et al.* (LIGO Scientific), Class. Quant. Grav. **32**, 074001 (2015), arXiv:1411.4547 [gr-qc].
- [11] A. Romero, K. Martinovic, T. A. Callister, H.-K. Guo, M. Martínez, M. Sakellariadou, F.-W. Yang, and Y. Zhao, Phys. Rev. Lett. **126**, 151301 (2021), arXiv:2102.01714 [hep-ph].
- [12] P. Amaro-Seoane *et al.* (LISA), (2017), arXiv:1702.00786 [astro-ph.IM].
- [13] W.-H. Ruan, Z.-K. Guo, R.-G. Cai, and Y.-Z. Zhang, (2018), arXiv:1807.09495 [gr-qc].
- [14] Z. Arzoumanian *et al.* (NANOGrav), Phys. Rev. Lett. **127**, 251302 (2021), arXiv:2104.13930 [astro-ph.CO].
- [15] X. Xue *et al.*, Phys. Rev. Lett. **127**, 251303 (2021), arXiv:2110.03096 [astro-ph.CO].
- [16] C. L. Carilli and S. Rawlings, *International SKA Conference 2003 Geraldton, Australia, July 27-August 2, 2003*, New Astron. Rev. **48**, 979 (2004), arXiv:astro-ph/0409274 [astro-ph].
- [17] M. D’Onofrio, K. Rummukainen, and A. Tranberg, Phys. Rev. Lett. **113**, 141602 (2014), arXiv:1404.3565 [hep-ph].
- [18] Z. Fodor and S. D. Katz, JHEP **03**, 014 (2002), arXiv:hep-lat/0106002.
- [19] L. Bian *et al.*, Sci. China Phys. Mech. Astron. **64**, 120401 (2021), arXiv:2106.10235 [gr-qc].
- [20] R.-G. Cai, Z. Cao, Z.-K. Guo, S.-J. Wang, and T. Yang, Natl. Sci. Rev. **4**, 687 (2017), arXiv:1703.00187 [gr-qc].
- [21] R. Caldwell *et al.*, Gen. Rel. Grav. **54**, 156 (2022), arXiv:2203.07972 [gr-qc].
- [22] D. J. Schwarz and M. Stuke, JCAP **11**, 025 (2009), [Erratum: JCAP 10, E01 (2010)], arXiv:0906.3434 [hep-ph].
- [23] M. M. Wygas, I. M. Oldengott, D. Bödeker, and D. J. Schwarz, Phys. Rev. Lett. **121**, 201302 (2018), arXiv:1807.10815 [hep-ph].
- [24] M. M. Middeldorf-Wygas, I. M. Oldengott, D. Bödeker, and D. J. Schwarz, Phys. Rev. D **105**, 123533 (2022), arXiv:2009.00036 [hep-ph].
- [25] F. Gao and I. M. Oldengott, Phys. Rev. Lett. **128**, 131301 (2022), arXiv:2106.11991 [hep-ph].
- [26] M. Breitbach, J. Kopp, E. Madge, T. Opferkuch, and P. Schwaller, JCAP **07**, 007 (2019), arXiv:1811.11175 [hep-ph].
- [27] P. D. Serpico and G. G. Raffelt, Phys. Rev. D **70**, 043526 (2004), arXiv:astro-ph/0403417.
- [28] X. Chu, J.-L. Kuo, and J. Pradler, Phys. Rev. D **106**, 055022 (2022), arXiv:2205.05714 [hep-ph].
- [29] N. Sabti, J. Alvey, M. Escudero, M. Fairbairn, and D. Blas, JCAP **01**, 004 (2020), arXiv:1910.01649 [hep-ph].
- [30] M. Escudero, JCAP **02**, 007 (2019), arXiv:1812.05605 [hep-ph].
- [31] N. Sabti, J. Alvey, M. Escudero, M. Fairbairn, and D. Blas, JCAP **08**, A01 (2021), arXiv:2107.11232 [hep-ph].
- [32] M. Escudero Abenza, JCAP **05**, 048 (2020), arXiv:2001.04466 [hep-ph].
- [33] Y. Bai and M. Korwar, Phys. Rev. D **105**, 095015 (2022), arXiv:2109.14765 [hep-ph].
- [34] S. R. Coleman, Phys. Rev. D **15**, 2929 (1977), [Erratum: Phys. Rev. D 16, 1248 (1977)].
- [35] K. Enqvist, J. Ignatius, K. Kajantie, and K. Rummukainen, Phys. Rev. D **45**, 3415 (1992).
- [36] S. He, L. Li, Z. Li, and S.-J. Wang, (2022), arXiv:2210.14094 [hep-ph].

- [37] M. S. Turner, E. J. Weinberg, and L. M. Widrow, Phys. Rev. **D46**, 2384 (1992).
- [38] M. Tanabashi *et al.* (Particle Data Group), Phys. Rev. D **98**, 030001 (2018).
- [39] E. W. Kolb and M. S. Turner, *The Early Universe*, Vol. 69 (1990).
- [40] N. Aghanim *et al.* (Planck), Astron. Astrophys. **641**, A6 (2020), [Erratum: Astron. Astrophys. 652, C4 (2021)], arXiv:1807.06209 [astro-ph.CO].
- [41] K. Ichikawa, M. Kawasaki, and F. Takahashi, Phys. Rev. D **72**, 043522 (2005), arXiv:astro-ph/0505395.
- [42] G.-y. Huang and W. Rodejohann, Phys. Rev. D **103**, 123007 (2021), arXiv:2102.04280 [hep-ph].
- [43] C. Pitrou, A. Coc, J.-P. Uzan, and E. Vangioni, Phys. Rept. **754**, 1 (2018), arXiv:1801.08023 [astro-ph.CO].
- [44] P. A. Zyla *et al.* (Particle Data Group), PTEP **2020**, 083C01 (2020).
- [45] C. Pitrou, A. Coc, J.-P. Uzan, and E. Vangioni, Mon. Not. Roy. Astron. Soc. **502**, 2474 (2021), arXiv:2011.11320 [astro-ph.CO].
- [46] A. G. Riess, S. Casertano, W. Yuan, L. M. Macri, and D. Scolnic, Astrophys. J. **876**, 85 (2019), arXiv:1903.07603 [astro-ph.CO].
- [47] N. Blinov, K. J. Kelly, G. Z. Krnjaic, and S. D. McDermott, Phys. Rev. Lett. **123**, 191102 (2019), arXiv:1905.02727 [astro-ph.CO].